ChemComm

COMMUNICATION

View Article Online
View Journal

Cite this: DOI: 10.1039/c8cc07886f

Received 3rd October 2018,
Accepted 12th December 2018

DOI: 10.1039/c8cc07886f

rsc.li/chemcomm

Size-selective encapsulation of C_{60} and C_{60}-derivatives within an adaptable naphthalene-based tetragonal prismatic supramolecular nanocapsule†

Cristina García-Simón, ‡*[a] Alba Monferrer,‡[a] Marc Garcia-Borràs, [b] Inhar Imaz, [c] Daniel Maspoch, [cd] Miquel Costas *[a] and Xavi Ribas *[a]

A novel naphthalene-based 5·$(BArF)_8$ capsule allows for the size-selective inclusion of C_{60} from fullerene mixtures. Its size selectivity towards C_{60} has been rationalized by its dynamic adaptability in solution that has been investigated by molecular dynamics. Additionally, 5·$(BArF)_8$ encapsulates C_{60}-derivatives such as C_{60}-PCBM and *N*-methylpyrrolidine-C_{60}. The latter can be separated from C_{60} since 5·$(BArF)_8$ displays distinct affinity for them.

The metal–ligand coordination approach has led to the preparation of sophisticated discrete three-dimensional (3D) structures, which are of great interest due to their intrinsic complexity, which conveys multifunctionality, and potential applications in fields such as molecular catalysis, sensing and purification.[1–3] Indeed, the possibility of tuning the dimensions of the confined space by modifying the 3D molecular structure is an attractive feature to gain control over the guest affinity, and allows for the preparation of extended libraries of coordination capsules.[4,5] On the other hand, the purification of fullerenes is remarkable due to their applications in materials science and medicine.[6,7] Even though fullerene extracts are easily available, the selective purification of a specific fullerene cage from a mixture of C_n ($n > 70$) cages is still a challenging task basically accomplished by means of high performance liquid chromatography (HPLC) techniques, which are generally tedious, time-consuming and energy consuming.[8] Another challenging issue is the purification of fullerene derivatives, which is also mainly restricted to HPLC separation. C_{60}-derivatives such as [6,6]-phenyl C_{61} butyric acid methyl ester (PCBM-C_{60}) and fulleropyrrolidines present promising applications in materials science, but they need to be available in a pure form to display full efficiency.[9,10] To date, numerous examples of 3D molecular receptors based on metal–ligand coordination bonds and capable of hosting fullerenes have been reported.[11–14] However, the separation of a single fullerene by size-confinement effects is not straightforward since the molecular receptors display high affinity for different-sized fullerenes simultaneously.[15] In most reported examples a higher affinity towards C_n ($n \geq 70$) over C_{60} is observed, due to the more significant solvophobic effects and the more extended π-surface of larger fullerenes that enhances capsule–fullerene interaction.[16–20] The reverse trend is observed in very limited examples.[21]

Our group previously reported a coordination nanocapsule (**4**·$(BArF)_8$) capable of encapsulating different-sized fullerenes from C_{60} to C_{84}.[22] This lack of size selectivity was attributed to its pronounced breathing ability and large cavity size. In light of the importance of C_{60} and its derivatives, herein we report a nanocapsule (**5**·$(BArF)_8$), which bears a smaller cavity, obtained by tuning the length of its spacers. The newly designed nanocapsule with naphthalene spacers is capable of exclusively encapsulating a smaller C_{60} fullerene and its corresponding mono-adduct derivatives in a selective manner.

New metallo-capsule **5**·$(X)_8$ (X = CF_3SO_3, BArF) was synthesized by coordination driven self-assembly of the carboxylate units from Zn^{II}-porphyrin (**2**) and Pd^{II}-based macrocyclic synthons (**Pd-1c**). **5**·$(X)_8$ differs from our previously reported capsules **3**·$(X')_8$ (X′ = ClO_4, CF_3SO_3) and **4**·$(X)_8$ in the nature of the hexaaza macrocyclic ligands used to synthesize ligands **1** and **1b** and therefore the corresponding Pd^{II}-clip building blocks (Scheme 1).[22,23] Nanocapsule **3**·$(X')_8$ contained a phenyl ring in its macrocyclic ligands (**1**), and the crystallographic distance between its porphyrins was 7.5 Å. On the other hand, **4**·$(X)_8$ included a biphenyl moiety in **1b**, rendering a Porph-Zn···Porph-Zn distance of 14.1 Å measured from the X-ray structure (Fig. 2). While the former capsule **3** was only capable of encapsulating

[a] *Institut de Química Computacional i Catàlisi (IQCC) and Departament de Química, Universitat de Girona, Campus Montilivi, Girona, E-17003, Catalonia, Spain. E-mail: cristina.simon@udg.edu, miquel.costas@udg.edu, xavi.ribas@udg.edu*

[b] *Department of Chemistry and Biochemistry, University of California, Los Angeles, CA90095, USA*

[c] *Institut Català de Nanociència i Nanotecnologia, ICN2, Campus UAB, 08193 Bellaterra, Catalonia, Spain*

[d] *ICREA, Pg. Lluís Companys 23, 08010 Barcelona, Catalonia, Spain*

† Electronic supplementary information (ESI) available. CCDC 1561152 and 1561153. For ESI and crystallographic data in CIF or other electronic format see DOI: 10.1039/c8cc07886f

‡ These authors contributed equally to this work.

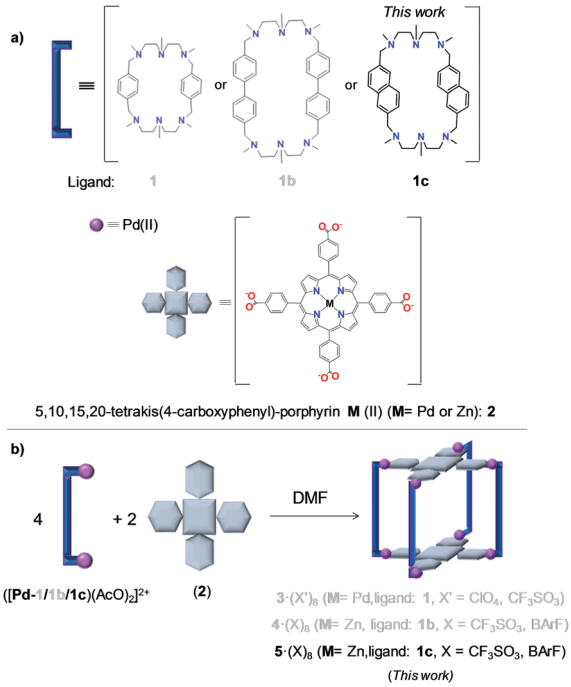

Scheme 1 Schematic representation of the library of coordination nanocapsules **3–5**. (a) Spacers used to obtain (b) the tetragonal-prismatic supramolecular capsules **3**·(X′)$_8$ (X′ = ClO_4, CF_3SO_3), **4**·(X)$_8$ and **5**·(X)$_8$ (X = CF_3SO_3, BArF) (BArF: tetrakis[3,5-bis(trifluoromethyl)phenyl]borate).

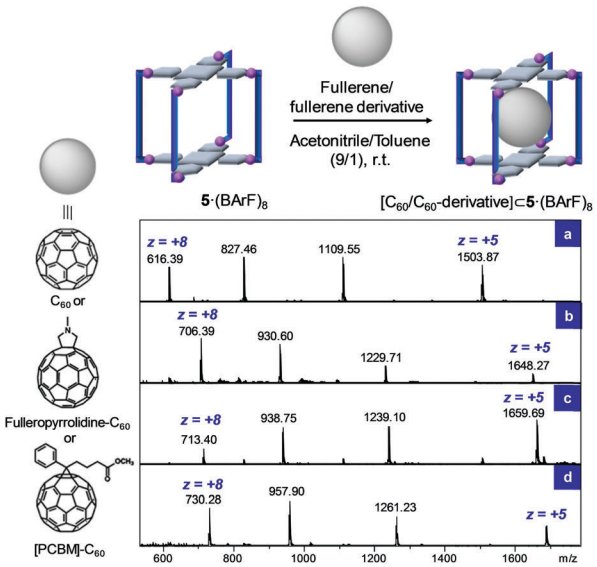

Fig. 1 HRMS of **5**·(BArF)$_8$ and its host–guest adducts. HRMS in CH_3CN of (a) **5**·(BArF)$_8$, (b) $C_{60}\subset$**5**·(BArF)$_8$, (c) [(mono)-*N*-pyrrolidine-C_{60}]$\subset$**5**·(BArF)$_8$ and (d) [PCBM-C_{60}]$\subset$**5**·(BArF)$_8$.

flat anionic π-guests, capsule **4** could host fullerene molecules up to C_{84} with very high association constants (up to $K_a > 10^8$ M^{-1}). For the new nanocapsule **5**·(X)$_8$, which contains 2,6-disubstituted naphthalene units in the macrocyclic ligand (**1c**) (Fig. S1–S27, ESI†), an intermediate capsule-size was envisioned (Scheme 1).

The formation of nanocapsule **5**·$(CF_3SO_3)_8$ was first confirmed by high-resolution mass spectrometry (HRMS) (Fig. S28, ESI†). Then, $CF_3SO_3^-$ anions were exchanged with BArF anions to increase its solubility. **5**·(BArF)$_8$ was obtained in good yield, effectively showing an enhanced solubility in different organic solvents, including CH_3CN and dichloromethane (DCM). HRMS of **5**·(BArF)$_8$ showed ions corresponding to the cages with a consecutive loss of counteranions (Fig. 1a and Fig. S29, ESI†), demonstrating its integrity in solution. Full NMR characterization was also performed for **5**·(BArF)$_8$ (Fig. S30–S36, ESI†). Remarkably, the DOSY NMR experiment (CH_3CN, 298 K) afforded a diffusion coefficient of $D = 3.1 \times 10^{-10}$ m^2 s^{-1}, indicating that the dimensions of $\mathbf{5}^{8+}$ correspond to a hydrodynamic radius of 18.5 Å in solution (Fig. S37 and S38, ESI†), in line with the value estimated from crystallographic data (see below and Fig. S38b, ESI†).

Crystallographic data were obtained from **5**·$(CF_3SO_3)_8$ crystals at the XALOC beamline of the ALBA Synchrotron (Fig. 2a and ESI† for Single-Crystal X-Ray Diffraction – SCXRD details). Nanocapsule $\mathbf{5}^{8+}$ consists of two parallel tetracarboxylated Zn^{II}-porphyrins linked by four macrocyclic dinuclear Pd^{II} complexes. The four-carboxylate residues of each porphyrin are linked by means of η^1-O monodentate coordination to one Pd^{II} center (Fig. S38, ESI†). As in $\mathbf{3}^{8+}$ and $\mathbf{4}^{8+}$,[19,20] $\mathbf{5}^{8+}$ presents a tetragonal prismatic geometry bearing D_4 symmetry. The crystallographic Porph-Zn···Porph-Zn distance in **5**·$(CF_3SO_3)_8$ is 8.2 Å. As expected, this distance lies between those observed in capsules **3**·(X′)$_8$ and **4**·(X)$_8$ (see Scheme 1 and Fig. 2a). In light of the size contraction with respect to **4**·(X)$_8$, it was predicted that **5**·(X)$_8$ will offer a higher affinity to smaller fullerenes.

Once **5**·(BArF)$_8$ was fully characterized, its ability to host fullerenes was tested starting with the encapsulation of C_{60}. Here, the fast formation of 1 : 1 host : guest adducts was observed after mixing a 1 : 1 molar solution of **5**·(BArF)$_8$ in CH_3CN and C_{60} in toluene. HRMS of the 1 : 1 C_{60} : **5**·(BArF)$_8$ mixture showed peaks corresponding exclusively to $C_{60}\subset$**5**·(BArF)$_8$ (Fig. 1b and Fig. S39, ESI†). Data obtained from the UV-Vis titration of C_{60} and **5**·(BArF)$_8$ fitted to a 1 : 1 binding model with an association constant of 1.29 (±0.42) × 10^5 M^{-1} (all UV-vis titrations were performed in a toluene/acetonitrile solvent mixture (9/1) and the host concentration was kept constant, Fig. S40, ESI†).[24] The formation of the host : guest adduct was also evidenced in the ^{1}H-NMR spectrum, which showed several signals shifted, especially those corresponding to the aromatic protons of the phenyl rings of the porphyrin pointing into the cavity (Fig. S41, ESI†).

Afterwards, the encapsulation of C_{70} was also attempted and monitored by HRMS. Remarkably, when a solution of C_{70} in toluene was mixed with a solution of **5**·(BArF)$_8$ in CH_3CN in a 2 : 1 molar ratio (298 K, 48 h), peaks corresponding to the $C_{70}\subset$**5**·(BArF)$_8$ adduct as well as peaks belonging to the remaining empty capsule were observed (3 : 2 ratio, respectively, see Fig. S42, ESI†). These results indicated a notable lower affinity of the capsule towards C_{70} compared to C_{60}. UV-Vis titration with C_{70} was in line with HRMS, since negligible changes in the Soret band were detected (Fig. S43, ESI†).

The encapsulation of C_{60} might seem surprising based solely on the short Porph-Zn···Porph-Zn distance measured in the

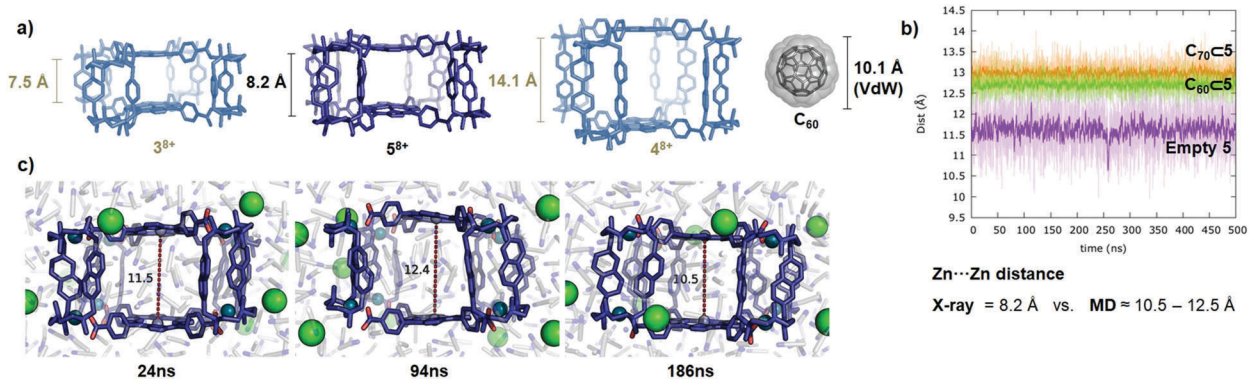

Fig. 2 Crystal structures of the library of capsules $\mathbf{3}^{8+}$–$\mathbf{5}^{8+}$ and illustrations of the MD simulation of capsule **5**. (a) Lateral views of the crystal structures of **3**·$(ClO_4)_8$, **4**·$(BArF)_8$ and **5**·$(CF_3SO_3)_8$ (counterions and hydrogen atoms are omitted for clarity). (b) Zn···Zn distance measured along the 500 ns of Molecular Dynamics (MD) trajectory for **5**·$(Cl)_8$ (purple), C_{60}⊂**5**·$(Cl)_8$ (green) and C_{70}⊂**5**·$(Cl)_8$ (orange) in explicit CH_3CN solvent. For more clarity, the 10-step averaged value for each point is represented by the purple line in the plot. (c) Representative snapshots taken along the MD trajectory to illustrate the conformational flexibility of $\mathbf{5}^{8+}$. Zn···Zn distances are given in Å, and hydrogen atoms are omitted for clarity.

crystal structure. This distance, 8.2 Å, is much smaller than the van der Waals diameter of C_{60} (10.1 Å), thus indicating that **5**·$(BArF)_8$ must undergo important structural changes in solution to be able to accommodate C_{60} (Fig. 2a). The latter was explored through molecular dynamics (MD) simulations using CH_3CN as explicit solvent and Cl^- as counterions (see the ESI† for details). MD simulations revealed that the Porph-Zn···Porph-Zn distance in empty **5**·$(Cl)_8$ swings from 10.5 to 12.5 Å in solution (Fig. 2b and c and Video VS1 in the ESI†). On the other hand, MD simulations on C_{60}⊂**5**·$(Cl)_8$ and C_{70}⊂**5**·$(Cl)_8$ host–guest complexes showed a Porph-Zn···Porph-Zn distance of 12.3–13 Å for the C_{60} system and 12.6–13.3 Å for the C_{70} system (Fig. S44, ESI†). Porph-Zn···Porph-Zn distances explored during the MD trajectory in C_{70}⊂**5**·$(Cl)_8$ are larger than the Porph-Zn···Porph-Zn distances measured in empty **5**·$(Cl)_8$ during MD, while C_{60}⊂**5**·$(Cl)_8$ distances are in the breathing range (Fig. 2b). Indeed, when comparing these Porph-Zn···Porph-Zn distances to those observed in the previously reported crystal structures of C_{60}⊂**4**·$(BArF)_8$ and C_{70}⊂**4**·$(BArF)_8$, 13.1 Å and 13.7 Å for C_{60} and C_{70}, respectively,[22] the idea that C_{70} fullerene imposes a more severe distortion on the nanocapsule **5** than C_{60} is reinforced. This large distortion of the nanocapsule **5** required to encapsulate C_{70} is in agreement with the hampered encapsulation of C_{70} within **5**·$(BArF)_8$ and the higher selectivity towards C_{60}.

Encapsulation experiments with C_{60} were also performed using **5**·$(CF_3SO_3)_8$ in the solid state. Interestingly, C_{60} was trapped after adding the solid capsule to a solution of the fullerene in toluene (1 : 8 capsule : fullerene molar ratio, a higher excess of fullerene was applied in the solid : liquid experiments to facilitate the less favoured encapsulation) (Fig. S45, ESI†). The full formation of the C_{60}⊂**5**·$(CF_3SO_3)_8$ adduct was observed after 1 h stirring. Note here that the liquid/liquid complexation occurs more rapidly (<5 min, 1 : 1 capsule : fullerene ratio) than the solid/liquid one. The slower rate of the solid/liquid encapsulation is most likely due to the higher rigidity of the capsule in the solid state, which restricts its dynamic adaptability needed to accommodate C_{60}, as revealed by MD simulations.

Taking advantage of the higher size-selectivity for C_{60}, nanocapsule **5**·$(BArF)_8$ was used to selectively separate C_{60} from fullerene extracts (extract composition: 70% C_{60}, 28% C_{70}, 2% higher fullerenes). To this end, a solution of **5**·$(BArF)_8$ in CH_3CN was mixed with a solution of the fullerene extract in toluene, in a 1 : 2 molar ratio (capsule : fullerenes). Delightfully, HRMS experiments showed that C_{60} was exclusively encapsulated from all the fullerene mixtures (Fig. S46, ESI†). No peaks corresponding to adducts with C_{70} or with other higher fullerenes present in the soot (*i.e.* C_{72}, C_{76} or C_{84}) were observed, even using extended reaction times. The same experiment was repeated using solid **5**·$(CF_3SO_3)_8$, in which C_{60} fullerene was also solely encapsulated (capsule : fullerene-extract in a 1 : 8 molar ratio, see Fig. S47, ESI†). In contrast, when a larger **4**·$(BArF)_8$ capsule is added, in either the solid or liquid form, to a fullerene extract solution, both C_{60} and C_{70} and other higher fullerenes are encapsulated, displaying no size exclusion.[22]

Finally, the ability of **5**·$(BArF)_8$ to encapsulate C_{60} derivatives was also explored. Host–guest studies were carried out with PCBM-C_{60} and *N*-methylpyrrolidine-C_{60} (the latter was prepared as previously reported).[25] When a solution of the corresponding derivative in toluene was mixed with a solution of the capsule in acetonitrile in a 1 : 1 molar ratio, a clean formation of the host–guest complexes was observed by HRMS after 5 min stirring (Fig. 1c and d and Fig. S48, 49, ESI†). UV-Vis titration experiments were performed in order to estimate the association constant between the **5**·$(BArF)_8$ receptor and the C_{60}-derivatives. Interestingly, the UV-Vis experiment following the formation of the [*N*-methylpyrrolidine-C_{60}]⊂**5**·$(BArF)_8$ complex gave an association constant of 6.60 ($\pm$0.32) $\times$ 10^4 M^{-1} (2-fold smaller than the one obtained for C_{60}, Fig. S50, ESI†) and the [PCBM-C_{60}]⊂**5**·$(BArF)_8$ complex gave an association constant of 1.27 ($\pm$2.04) $\times$ 10^5 M^{-1} (Fig. S51, ESI†), which is very similar to the one obtained for C_{60}. Encapsulation of both functionalized fullerenes was also performed using the **5**·$(CF_3SO_3)_8$ capsule in the solid state. Both species showed complete encapsulation after 1 h stirring a capsule suspension in a fullerene-derivative toluene solution (Fig. S52 and S53, ESI†); however, encapsulation

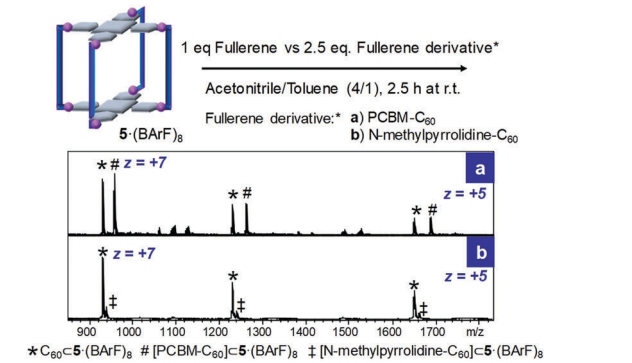

Fig. 3 HRMS spectra of the competition experiments of (a) C_{60} *vs.* PCBM-C_{60} and (b) C_{60} *vs. N*-methylpyrrolidine-C_{60}.

of PCBM-C_{60} was faster as was evidenced by the HRMS spectrum recorded after 30 min reaction time compared to the one obtained for *N*-methylpyrrolidine-C_{60} (Fig. S52 and S53, ESI†). The latter observation is in agreement with the higher association constant obtained for PCBM-C_{60}.

A competition experiment between C_{60} fullerene and the PCBM-C_{60} derivative further supports the similar values obtained for their association constants. When 1 equivalent of the **5**·$(BArF)_8$ capsule was mixed with 2.5 eq. of C_{60} and 2.5 eq. of PCBM-C_{60}, in toluene/acetonitrile (4/1) for 2.5 h, very similar intensity peaks on the HRMS were observed in line with the similar K_a values (see Fig. 3a and Fig. S54, ESI†). Interestingly, when an analogous experiment was performed using *N*-methylpyrrolidine-C_{60} instead of PCBM-C_{60}, selective encapsulation of C_{60} occurred. In the latter case, the HRMS spectrum of the crude material displayed peaks corresponding to the $C_{60}\subset$**5**·$(BArF)_8$ adduct and only residual peaks corresponding to the *N*-methylpyrrolidine-$C_{60}\subset$**5**·$(BArF)_8$ adduct (Fig. 3b and Fig. S55 and S56 for comparable ionization behaviors in HRMS, ESI†). The notable difference between the association constants of C_{60} and the C_{60}-fulleropyrrolidine derivative ($K_a(C_{60})/K_a(C_{60}$-fulleropyrrolidine) $\sim$2) also enabled the separation of mono-Prato-C_{60} using a previously described solid-washing strategy.[22] When a solid sample of **5**·$(BArF)_8$ containing both C_{60} and *N*-methylpyrrolidine-C_{60} was washed with CS_2, the Prato derivative was released, while the C_{60} fullerene remained trapped within the nanocapsule (see Fig. S57, ESI†).

In summary, contraction of the length of the organic macrocyclic ligands of the previously described **4**·$(BArF)_8$ capsule by changing biphenyl subunits for naphthalene led to the new tetragonal prismatic nanocapsule **5**·$(BArF)_8$. Remarkably, the size-selectivity imposed by the anisotropically contracted nanocapsule allows for the selective separation of C_{60} from fullerene extract mixtures. Its capacity to host fullerenes and its size selectivity towards C_{60} can be rationalized by the dynamic adaptability that the capsule structure displays in solution, as shown by MD simulations. **5**·$(BArF)_8$ also encapsulates C_{60}-PCBM and *N*-methylpyrrolidine-C_{60}, displaying a larger affinity for C_{60} than for the latter Prato derivative, allowing its selective purification. Nanocapsule **5**·$(BArF)_8$ sets the knowledge basis for future purification of C_{60}-derivative mixtures.

This work was supported by MINECO-Spain (CTQ2016-77989-P to X. R., CTQ2015-70795-P to M. C., MAT2015-65354-C2-1-R to D. M. and I. I., 2017 SGR 264 to X. R., and 2014SGR80 to D. M.), the CERCA Programme/Generalitat de Catalunya, ICREA-Acadèmia (X. R. and M. C.), the Ramón Areces Foundation (M. G.-B.) and the Severo Ochoa Center of Excellence Program (ICN2, Grant SEV-2017-0706).

Conflicts of interest

There are no conflicts to declare.

Notes and references

1 C. García-Simón, R. Gramage-Doria, S. Raoufmoghaddam, T. Parella, M. Costas, X. Ribas and J. N. H. Reek, *J. Am. Chem. Soc.*, 2015, **137**, 2680–2687.
2 C. Zhao, F. D. Toste, K. N. Raymond and R. G. Bergman, *J. Am. Chem. Soc.*, 2014, **136**, 14409–14412.
3 K. Yamashita, M. Kawano and M. Fujita, *Chem. Commun.*, 2007, 4102–4103.
4 T. R. Cook, Y.-R. Zheng and P. J. Stang, *Chem. Rev.*, 2013, **113**, 734–777.
5 J. J. Henkelis and M. J. Hardie, *Chem. Commun.*, 2015, **51**, 11929–11943.
6 H. W. Kroto, J. R. Heath, S. C. O'Brien, R. F. Curl and R. E. Smalley, *Nature*, 1985, **318**, 162–163.
7 J. J. Ryan, H. R. Bateman, A. Stover, G. Gomez, S. K. Norton, W. Zhao, L. B. Schwartz, R. Lenk and C. L. Kepley, *J. Immunol.*, 2007, **179**, 665–672.
8 J. Xiao and M. E. Meyerhoff, *J. Chromatogr. A*, 1995, **715**, 19–29.
9 Y. Matsuo, A. Iwashita, Y. Abe, C. Li, K. Matsuo, M. Hashiguchi and E. Nakamura, *J. Am. Chem. Soc.*, 2008, **130**, 15429–15436.
10 G. Dennler, M. C. Scharber and C. J. Brabec, *Adv. Mater.*, 2009, **21**, 1323–1338.
11 C. Garcia-Simon, M. Costas and X. Ribas, *Chem. Soc. Rev.*, 2016, **45**, 40–62.
12 M. Zhang, H. Xu, M. Wang, M. L. Saha, Z. Zhou, X. Yan, H. Wang, X. Li, F. Huang, N. She and P. J. Stang, *Inorg. Chem.*, 2017, **56**, 12498–12504.
13 C. Colomban, G. Szalóki, M. Allain, L. Gómez, S. Goeb, M. Sallé, M. Costas and X. Ribas, *Chem. – Eur. J.*, 2017, **23**, 3016–3022.
14 T. K. Ronson, W. Meng and J. R. Nitschke, *J. Am. Chem. Soc.*, 2017, **139**, 9698–9707.
15 K. Tashiro and T. Aida, *Chem. Soc. Rev.*, 2007, **36**, 189–197.
16 W. Meng, B. Breiner, K. Rissanen, J. D. Thoburn, J. K. Clegg and J. R. Nitschke, *Angew. Chem., Int. Ed.*, 2011, **50**, 3479–3483.
17 C. Zhang, Q. Wang, H. Long and W. Zhang, *J. Am. Chem. Soc.*, 2011, **133**, 20995–21001.
18 V. Martínez-Agramunt, D. G. Gusev and E. Peris, *Chem. – Eur. J.*, 2018, **24**, 14802–14807.
19 Y. Shi, K. Cai, H. Xiao, Z. Liu, J. Zhou, D. Shen, Y. Qiu, Q. Guo, C. Stern, M. R. Wasielewski, F. Diederich, W. A. Goddard and J. F. Stoddart, *J. Am. Chem. Soc.*, 2018, **140**, 13835–13842.
20 S. Kawano, T. Fukushima and K. Tanaka, *Angew. Chem., Int. Ed.*, 2018, **1**, 14827–14831.
21 N. Kishi, Z. Li, K. Yoza, M. Akita and M. Yoshizawa, *J. Am. Chem. Soc.*, 2011, **133**, 11438–11441.
22 C. García-Simón, M. Garcia-Borràs, L. Gómez, T. Parella, S. Osuna, J. Juanhuix, I. Imaz, D. Maspoch, M. Costas and X. Ribas, *Nat. Commun.*, 2014, **5**, 5557.
23 C. García-Simón, M. Garcia-Borràs, L. Gómez, I. Garcia-Bosch, S. Osuna, M. Swart, J. M. Luis, C. Rovira, M. Almeida, I. Imaz, D. Maspoch, M. Costas and X. Ribas, *Chem. – Eur. J.*, 2013, **19**, 1445–1456.
24 D. Brynn Hibbert and P. Thordarson, *Chem. Commun.*, 2016, **52**, 12792–12805.
25 M. Maggini and M. Prato, *J. Am. Chem. Soc.*, 1993, **115**, 9798–9799.

